# Nanoscale investigation of vertically aligned carbon nanotube bundles for enhanced thermal management applications

Jean Spièce,[1,2] Kunal Lulla,[2,3] Pauline de Crombrugghe de Picquendaele,[1] Laurent Divay,[4] Odile Bezencenet,[4] Benoit Hackens,[1] Pascal Gehring,[1] Alex J. Robson,[2] Charalambos Evangeli,[2,5] and Oleg V. Kolosov[2]

[1)] *IMCN/NAPS, UCLouvain, B-1348 Louvain-la-Neuve, Belgium*

[2)] *Physics Department, Lancaster University, LA1 4YB, Lancaster, UK*

[3)] *National Graphene Institute, The University of Manchester, M13 9PL, Manchester, UK*

[4)] *Thales Research and Technology, 1, Avenue Augustin Fresnel, 91767 Palaiseau, France*

[5)] *Department of Materials, University of Oxford, Parks Road, OX1 3PH, Oxford, UK*

(*Electronic mail: ch.evangeli@gmail.com)

(*Electronic mail: jean.spiece@uclouvain.be)

Electronic devices continue to shrink in size while increasing in performance making excess heat dissipation challenging. Traditional thermal interface materials (TIMs) like thermal grease and pads face limitations in thermal conductivity and stability, particularly as devices scale down. Carbon nanotubes (CNTs) have emerged as promising candidates for TIMs thanks to their exceptional thermal conductivity and mechanical properties. However, the thermal conductivity of CNT films decreases when integrated into devices due to defects and bundling effects. This study employs a novel cross-sectional approach combining High Vacuum Scanning Thermal Microscopy (SThM) with Beam Exit Cross-Sectional Polishing (BEXP) to investigate the nanoscale morphology and thermal properties of vertically aligned CNT bundles at low and room temperature. Using appropriate thermal transport models, we extracted effective thermal conductivities of the vertically aligned nanotubes and obtained 4 $Wm^{-1}K^{-1}$ at 200 K and 37 $Wm^{-1}K^{-1}$ at 300 K. Additionally, non-negligible lateral thermal conductance between CNT bundles suggests complex heat transfer mechanisms within the sample. These findings provide unique insights into nanoscale thermal transport in CNT bundles, crucial for optimizing novel thermal management strategies.

## INTRODUCTION

While the size of electronic components is decreasing and their performance is increasing, the dissipation of excess heat is becoming a major issue for their development. This requires connecting the heat spreader of a device to the active electronic components, which can be challenging due to the device architecture, hot spots multiplications or ill-defined surfaces. Thermal interface materials (TIMs), including thermal grease, conductive adhesives and thermal pad, are used to fill this gap between two materials.[1,2] However, these materials due to their low thermal conductivity and stability, are problematic when scaling down the devices.[3,4] For the last decades, carbon nanotubes (CNTs) have attracted great research effort for their application as TIMs thanks to their high thermal conductivity, mechanical properties and operating stability.[4–9]

The thermal conductivity of a single isolated CNT reaches very high values, in the order of a few 1000 $Wm^{-1}K^{-1}$.[10,11] However, it dramatically decreases when several CNTs are integrated in films for potential TIM applications. Defects arising from the CNTs themselves, impurities, their length and coupling are responsible for increasing phonon scattering and thus, decreasing the effective thermal conductivity of the material.[12] High-density vertically aligned CNTs have demonstrated a superior pathway for thermal management applications.[4,13] Nevertheless, in such configuration, CNTs tend to aggregate and form bundles which affect their thermal characteristics.[14] For example, increasing the bundle size decreases significantly the thermal conductivity compare to a single CNT.[15,16]

Using CNTs in TIMs preparation involves several manufacturing steps which drastically changes the morphology and properties of its constituents. A precise knowledge of their nanoscale morphology and thermal properties is crucial for improving their functionality. Usual cross-sectional tools such as Focused Ion Beam and TEM investigations, which are suitable for such studies, require long and costly preparations.

To overcome these challenges, we exploited the unique ability of cross-sectional Scanning Thermal Microscopy. This method combines a universal polishing approach, Beam Exit Cross-Sectional Polishing (BEXP)[17] with Scanning Thermal Microscopy.[18,19] Here, BEXP creates a shallow angle beveled layer of vertically aligned CNTs with increasing length suitable for Atomic Force Microscopy (AFM) based techniques as well as Scanning Electron Microscopy (SEM) and Raman spectroscopy. Over other cross-sectioning tools that create tiny polished regions, BEXP has the advantage of unveiling the sample internal morphology from substrate to top. This allowed us to gain morphological, mechanical and thermal properties of the cross-sectioned CNTs. We observed bundles with 24 nm mean diameter and $28 \pm 2\%$ substrate coverage. Moreover, we studied the thermal transport of CNTs with varying length at room and cryogenic temperatures by high vacuum scanning thermal microscopy (SThM). Interestingly, we found that diffusive thermal transport mechanism is dominating in the vertically aligned CNTs bundles, even in short length bundles, with an effective thermal conductivity of 4 $Wm^{-1}K^{-1}$ at 200 K and increased to 37 $Wm^{-1}K^{-1}$ at 300 K. Our results are confirmed by Raman spectroscopy showing that the sample is highly disordered across the whole CNTs layer.

## SAMPLE PREPARATION AND CHARACTERISATION TECHNIQUES

A forest of vertically aligned carbon nanotubes was grown on a silicon substrate. The nanotubes were synthesized using chemical vapour deposition as reported elsewhere.[20] The process requires a seed layer composed of iron catalyst on top of an aluminium oxide barrier.

After growth, the sample is polished by beam-exit cross-sectional polishing - BEXP[17,18] (Fig. 1(a)). This nano-cross-sectioning tool creates an easily accessible wedge spanning through the whole 3D-structure of the sample uncovering subsurface features of the studied materials. BEXP uses three intersecting Ar-ion beams aligned to a single plane that impinge the sample at a small negative angle ($\sim -5°$) from below the sample surface. Even though the BEXP method has been already applied to numerous materials[17,18,21,22], we demonstrate here that it can also be applied to highly anisotropic materials and even non-fully covered surfaces.

For structural characterization, SEM imaging and Raman spectroscopy were employed. Nanomechanical characterisation is performed with Ultrasonic Force Microscopy (UFM), an AFM based technique highly sensitive to surface and subsurface structures of different materials.[23–27]

Finally, to thermally characterise the CNTs forest, we use cross-sectional Scanning Thermal Microscopy in high vacuum, both at room (300 K) and cryogenic temperatures (200 K).[18,28] SThM is a scanning probe technique where a micromachined AFM cantilever with a temperature sensor close to the tip is used to map the thermal transport in the sample. The tip highly resistive component acts as both a heating element and a temperature sensor. Thus, by monitoring the electrical resistance while raster scanning the sample, a thermal resistance map can be extracted.[28,29]

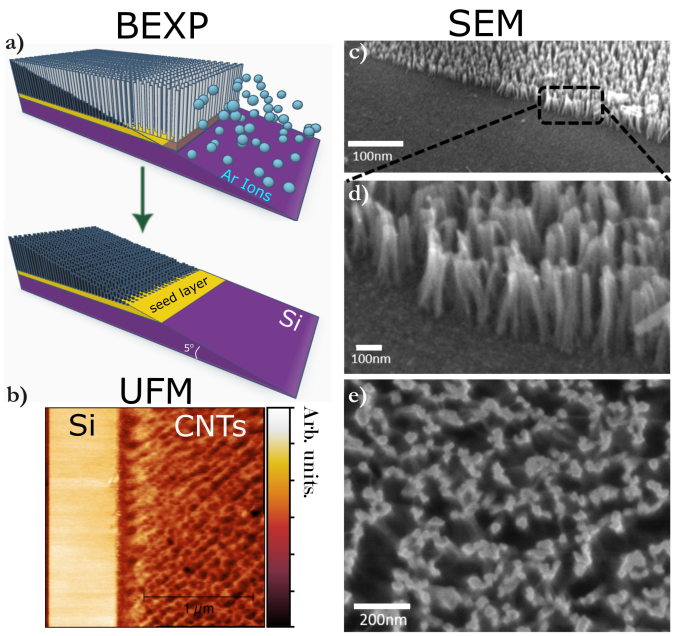


FIG. 1. (a) Schematics of beam-exit cross-sectional polishing - BEXPs technique. (b) UFM map of the silicon-nanotubes interface. Note that, stiffer areas are represented by brighter colours. (c,d) SEM images of the nanotubes bundles with increasing height (c), and a zoom in image at the same area (d). Bundles can be observed to form directly on the growth substrate. (e) Top view SEM image showing $28 \pm 2\%$ coverage of CNTs.

## RESULTS AND DISCUSSION

In Fig. 1(c-d), SEM images of an array of vertically aligned CNTs with increasing height after cross-sectioning the sample are shown. Part of the sample was shaved off with an AFM tip to observe the CNTs from their side. Individual tube can hardly be seen due to the SEM resolution. Interestingly, the vertical alignment is not affected by the BEXP process. However, as observed in Fig. 1(d), the CNTs form bundles consisting of several individual aggregated CNTs. The bundling effect begins directly at the seed layer and the average bundle diameter is 24 nm corresponding to approximately 3 nanotubes bundled together. From SEM imaging (see Fig. 1(e)), we estimate the CNT coverage to $28 \pm 2\%$.

In Fig. 1(b), an UFM map is shown, providing a nanomechanical understanding of the sample. A stronger signal corresponds to a stiffer material and, as it can be expected, the silicon substrate is stiffer than the nanotubes bundles. Indeed, as the CNTs bending stiffness is low due to their flexibility, they deform easily under the UFM indentation. We note also that this low stiffness along the tubes axis also impacts the SThM measurements of long bundles, as we show later. Indeed, long bundles of over few hundred nanometers become very floppy and hard to image with any contact mode measurement technique. This limits our analysis to tubes shorter than 250 nm.

In Fig. 2(a),(b), topography and thermal resistance images of the cross-sectioned area, obtained simultaneously in high vacuum at 300 K are presented. The silicon substrate and the seed layer appear less thermally resistive compared to the CNTs layer. While the lower thermal resistance of Si could be unexpected at first because of the lower Si thermal conductivity[30], there are two possible explanations for this observation. First, it is likely that the thermal contact between the silicon probe and the silicon is better than the one between the probe and the bundles. Second, the SThM probe is sensitive to the heat spreading resistance, not directly to the thermal conductivity. Thus, on one hand, the bundles, or any layer, act as an extra resistance between the sensor and the sample heat sink and, on the other hand, the bundles provide less material for heat spreading than the silicon substrate.

The topography and SThM images of the CNTs forest (see Fig. 2(c-f)) confirm the bundle effect. The topography images show a distribution of bundle sizes in agreement with the SEM measurements. Furthermore, a dip is obtained between the bundles highlighting the sharpness of the probe used. The lower thermal resistance between the bundles is due to an increased contact area between the tip and the sample. As individual bundles are resolved both in topography and SThM maps, we deduce that the tip-sample contact diam-

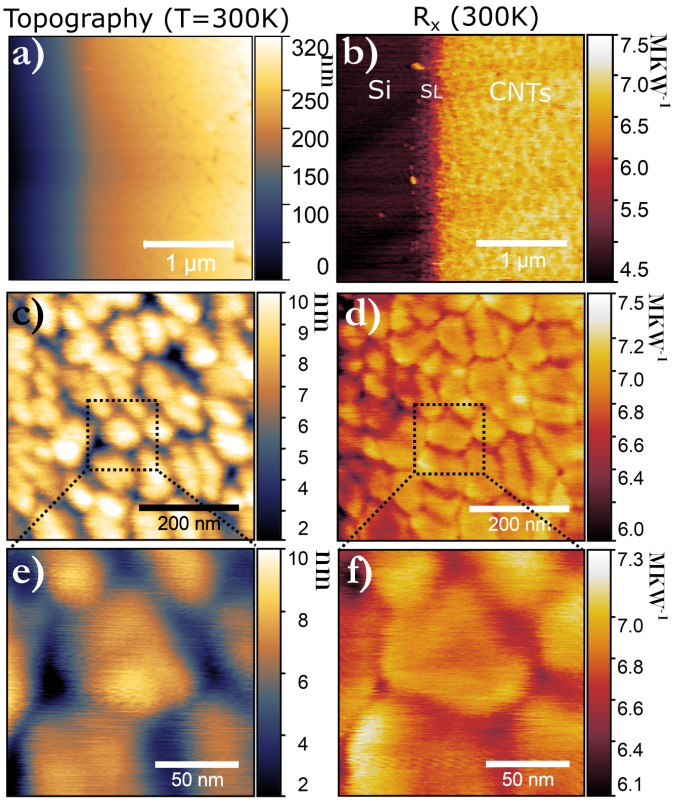


FIG. 2. (a-f) Topography (a,c,e) and thermal resistance (b,d,f) maps of the cross-sectioned area at T=300 K. Maps (e) and (f) are zoom in maps (c) and (d), respectively, and maps (c) and (d) zoom in maps (c) and (d), respectively. In (a) silicon, seed layer (SL) and the CNTs are shown.

eter is smaller than the bundle diameter.

To compare the thermal transport of CNTs at room- and low- temperatures, we extract from the topography and SThM images the thermal resistance profiles along the cross-sectioned area as function of the bundle height $t$ at 200 and 300 K (see Fig. 3(c) and (d)). The height is quantified from the topography since the thickness of the layer varies linearly with the position (see also SI). The x-axis origin is located at the beginning of the vertically aligned CNTs layer for convenience. Hence, negative heights correspond to material below the nanotubes. For both temperatures, the measured thermal resistance initially increases sharply for short nanotubes and then gradually saturates for longer CNTs. Comparing the two temperatures, we observe a giant increase in thermal resistance of CNTs, almost one order of magnitude at 200 K. An increase in the measured thermal resistance of Si substrate is also observed which was previously attributed to the increased Si phonon mean free path at low temperatures.[28]

The saturation of the thermal resistance for longer CNTs is related to the SThM sensitivity and indicates the sensitivity limit of the SThM.[31] At 300 K the thermal resistance saturates for CNTs longer than 75 nm, whereas at 200 K at almost at 150 nm, indicating an increased SThM sensitivity at lower temperatures.[28]

CNTs are attracting industrial interests for their intrinsically high thermal conductivity. However, high thermal conductivity values occur in pristine sample and isolated tubes. These high values mean that the phonon mean path can reach length as long as $1\mu$m.[32] Ballistic transport has been observed in stand-alone individual CNTs with lengths comparable to the phonon mean free path.[33] In our case, both bundling effect and inter-bundle contact as well as the temperature regime of the experiment are expected to increase phonon scattering processes, therefore greatly reducing the phonon mean free path ($l$).[34–36] However, at lower temperatures, the $l$ in CNTs is expected to increase.[36] A simple way to account for mixed ballistic-diffusive transport is to add both components as in $R = R_{\text{ballistic}} + R_{\text{diffusive}}$[37] or equivalent write[38,39]

$$R = R_{\text{ballistic}}(1 + \frac{L}{l}). \tag{1}$$

Thermal transport is ballistic when $l >> L$ and thermal conductivity increases linearly with the length, while thermal resistance remains constant. When $l < L$ diffusive transport contribution becomes more important and finally for very large $l << L$ it dominates. For diffusive transport, the thermal conductivity becomes length independent while thermal resistance increases with length. Considering that $R_{\text{tip}} + R_{\text{int}}$ is constant for different lengths, the evolution of $R_{\text{X}}$ with $L$ can give information for the transport nature in our system. The overall increase of $R_{\text{X}}$ with length for CNTs longer than 15 nm indicates a dominating diffusive transport contribution. The diffusive nature of the transport for CNTs is also supported by an additional modeling procedure we applied to our data (see SI).

To quantitatively extract the thermal properties of the CNTs, we consider a diffusive thermal transport mechanism. We express $R_{\text{X}}$ as a sum of thermal resistances of the conical tip itself $R_{\text{tip}}$, the tip apex-sample interface ($R_{\text{int}}$) and the spreading resistance inside the sample $R_{\text{spr}}$ (see also Fig. 3(a)):

$$R_{\text{X}} = R_{\text{tip}} + R_{\text{int}} + R_{\text{spr}}. \tag{2}$$

$R_{\text{tip}}$ is expected to be constant for all the different parts of the sample while $R_{\text{int}}$ is likely to change drastically between the tip-Si substrate and the tip-nanotubes contacts as previously discussed. However, we can assume that while scanning within the same material, for example, the nanotubes only, $R_{\text{int}}$ remains constant and therefore the sum $R_{\text{tip}} + R_{\text{int}}$ can be considered constant.

We apply two different diffusive transport models describing $R_{\text{spr}}$ of the cross-sectioned CNTs, namely 1D and orthotropic, respectively. The first model considers the sample as an array of vertically aligned cylinders and assumes one dimensional (1D) transport along these cylinders. The thermal resistance can be written as a function of the bundle height $L_{\text{bundle}}$:

$$R_{\text{bundle}} = \frac{L_{\text{bundle}}}{k_{\text{bundle}} A}, \tag{3}$$

where $A$ and $k_{\text{bundle}}$ is the cross-sectional area and the thermal conductivity of the bundle, respectively. Cross-sectional

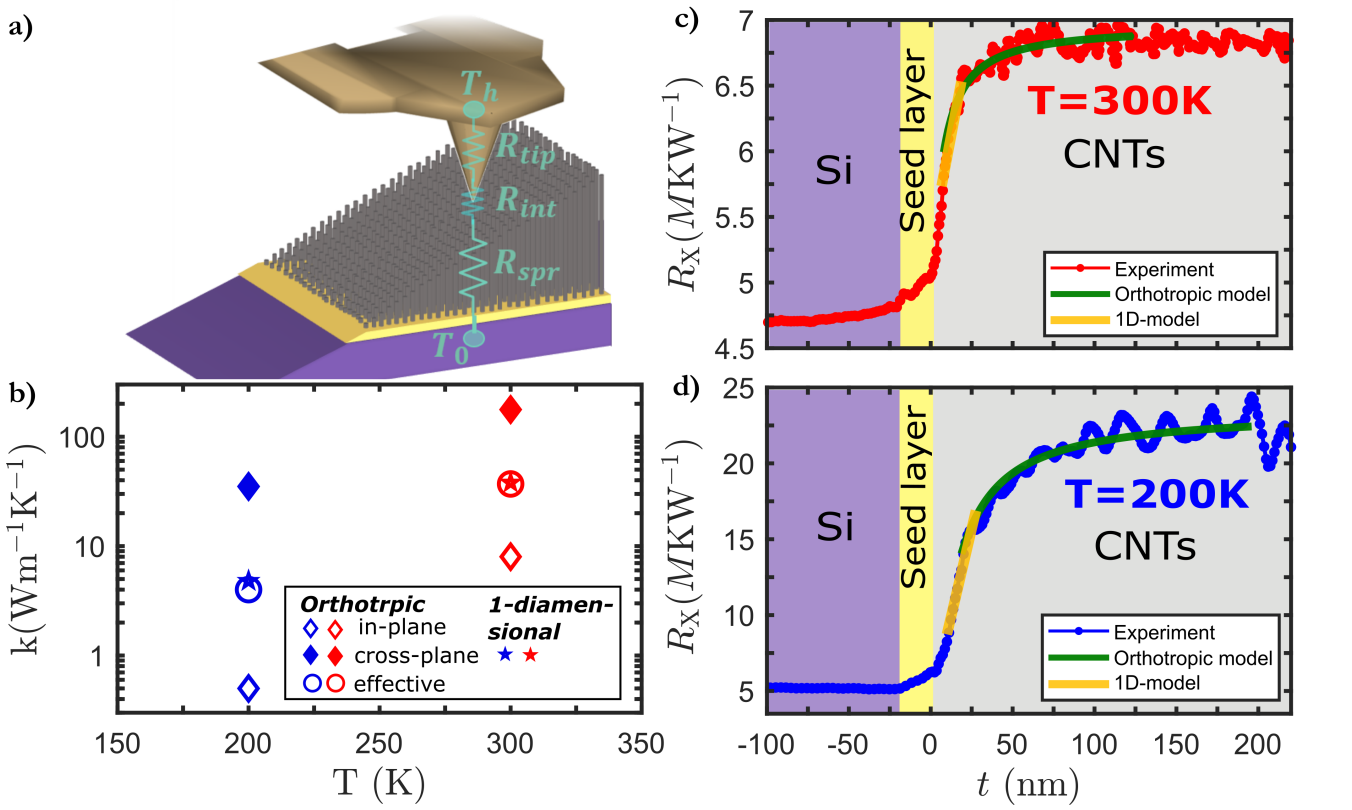


FIG. 3. (a) Schematics of thermal circuit with the resistances included between the sensor and the heat sink. $T_h$ is the tip-heater and $T_0$ the sample temperature, respectively. (b) Thermal conductivity values as obtained with the two models for different temperatures. (c,d) Thermal resistance measured as a function of nanotubes height ($t$) at room (c) and low (d) temperature, and fitting of the the two models applied. The $R_X$ profiles are acquired from the SThM image by averaging 100 lines as a function of height in the direction shown by the green arrow at Fig. 2(b) (see also SI for images at low temepratures).

area is ill-defined in the case of a single nanotube and thus for nanotube bundles.[40] For a single tube, it can be defined as $A = \pi d\delta$ with $d$ being the tube diameter and $\delta$ the layer separation of graphite. However, as in our case we are dealing with bundles, we consider the bundles as isotropic materials and as such we find a lower bound of the thermal conductivity.[41]

$R_X$ saturates for longer CNTs (at around 75 nm and 150 nm for 200 and 300 K, respectively), highlighting the fact that heat spreading also occurs perpendicularly to the CNT axis. Therefore, to model our samples as an array of cylinders, we use only the transition part between $10-30$ nm (see yellow line in Fig. 3(c) and (d)). It has been shown that the thermal conductivity of a single nanotube, saturates when it reaches 15 nm long.[34] Considering this region, we obtained a roughly linear trend with the height on the tubes, the derivative of the thermal resistance measured should compare to $dR_{\text{bundle}}/dL$. More importantly, this derivative does not depend on the tip-sample interface resistance ($R_{\text{tip}} + R_{\text{int}}$), contact area and interface contact resistance at the tubes-substrate interface.

The second model considers anisotropic heat transport in the CNTs area, with high thermal conductivity along the bundle axis, $k_{\parallel}$ and a low thermal conductivity perpendicularly, $k_{\perp}$. This allows us to use a model for $R_{\text{spr}}$ of layered material on a substrate and for a heat source of radius $a$.[42] In particular, it transforms the directional-dependent thermal conductivities $(k_{\perp}, k_{\parallel})$ of the layer to an effective isotropic thermal conductivity ($k_{\text{eff}}$) which includes the layer-substrate interface resistance ($r_{\text{int}}$) with thickness ($t_{\text{eff}}$) larger than the real thickness of the layer.[43] Finally $R_{\text{spr}}$ is given by

$$R_{\text{spr}}(t) = \frac{1}{\pi k_{\text{eff}} a}\int_0^{\infty}\left[\frac{1+K\exp\left(\frac{-2\xi t_{\text{eff}}}{a}\right)}{1-K\exp\left(\frac{-2\xi t_{\text{eff}}}{a}\right)}\right] J_1(\xi)\sin(\xi)\frac{d\xi}{\xi^2},. \tag{4}$$

where $\xi$ is the Bessel function, $k_{\text{eff}} = \sqrt{(k_{\perp}/k_{\parallel})}$ and $t_{\text{eff}} = \sqrt{(k_{\parallel}/k_{\perp})}t + r_{\text{int}}k_{\text{eff}}$, and $K = \frac{1-k_{\text{sub}}/k_{\text{eff}}}{1+k_{\text{sub}}/k_{\text{eff}}}$, with $k_{\text{sub}}$ being the substrate thermal conductivity.

We estimate a tip-sample contact diameter of $8 \pm 4$ nm, from the resistance measured on the silicon substrate (see SI for details). We fit the experimental data with $R_{\text{tip}} + R_{\text{int}}, r_{\text{int}}, k_{\text{perp}}, k_{\parallel}$ being the fitting parameters (see green line in Fig. 3(c) and (d)). Note, that this model considers a uniform layer on a substrate which is not the the case of the CNT layer, as bundles are not fully covering the surface. Therefore, $r_{\text{int}}$ and $k_{\parallel}$ need to be normalized to the CNTs coverage

($28 \pm 2\%$). However, this normalization is not necessary, for the one-dimensional heat transport, in which we considered that the tip contacts a single bundle and measures a resistance variation from the bundle length change.

The thermal conductivity values obtained with the two models are summarized in Fig. 3(b) and explicitly written in the SI. We find a good agreement of $k_{\text{bundle}}$ and $k_{\text{eff}}$ as obtained by the 1D- and the orthotropic model, respectively. The slightly higher values along the bundle axis for the orthotropic model at both temperatures is coherent as perpendicular transport is also considered in this model. Comparing the values for the 2 different temperatures, we see that the ones obtained at 200 K are lower than the ones obtained at room temperature. The increased thermal conductivity with temperature at this range is in line with previous works. At low temperatures, thermal conductivity increases with temperature due to the activation of additional phonon modes up to reach a maximum value around room temperature. For higher temperatures it decreases due to increased scattering.[10,40,44] Another observation is that thermal conductivity anisotropy decreases with temperature. This effect could be related to the decay of the mechanical properties of the CNTs at higher temperatures.[45]

Finally, we compare the thermal conductivity values obtained in this work with the ones in the literature for similar CNTs bundles. Overall, our values are smaller than ones reported for bundles of similar diameter. Feng et al. reported thermal conductivities of 100 and 110 $\text{Wm}^{-1}\text{K}^{-1}$ at $T = 200$ and 300 K, respectively for a bundle of 13 nanotubes and 450 and 1600 $\text{Wm}^{-1}\text{K}^{-1}$ for a 3 CNT bundles at the same temperatures .[15] Shi et al. on the other hand for 10 nm diameter bundle reported 130 and 215 $\text{Wm}^{-1}\text{K}^{-1}$ for $T = 200$ and $T = 300$ K, respectively.[16] Furthermore, for bundle of diameter 10.3 nm and 14.3$\mu$m length the thermal conductivity is found to be 253 $\text{Wm}^{-1}\text{K}^{-1}$.[46] Theoretical simulations predicted values ranging from 950 $\text{Wm}^{-1}\text{K}^{-1}$ and 5.6 $\text{Wm}^{-1}\text{K}^{-1}$[47] to 0.55 $\text{Wm}^{-1}\text{K}^{-1}$ and 0.028 $\text{Wm}^{-1}\text{K}^{-1}$[48] along and across the bundle, respectively. The lower values we observe, in comparison to the literature can be attributed to increased phonon scattering inside the CNT bundles and between the bundles. This is confirmed by the Raman spectrum measured in the cross-sectioned area, showing a high level of disorder in the sample compared to high quality crystalline nanotubes (see Supplementary Information section 4) .

## CONCLUSIONS

In conclusion, we performed thermal transport measurements on a unique sample composed of length increasing CNT bundles at high vacuum at 200 and 300 K. The sample was prepared by BEXP allowing shallow angle polishing. As the nanotubes kept their structure and alignment after the polishing, this opens new perspectives of materials study. A drastic increase in the thermal resistance with reducing temperature was measured which is related to the reducing CNT thermal conductivity. Two coherent diffusive modelling procedures were applied and obtained an effective thermal conductivity of 4 and 37$\text{Wm}^{-1}\text{K}^{-1}$ at 200 and 300 K. The thermal anisotropy was estimated using an orthotropic model accounting for the thermal conductivity along and perpendicular to the bundle axis taking into account the measured CNT coverage of the sample. Significantly, we found non negligible lateral thermal conductance between the nanotubes bundles. This study presents a new perspective for investigating vertical structures. It also provides information on the temperature dependence of the nanoscale thermal transport of vertically aligned CNT bundles.

## ACKNOWLEDGMENTS

O.K., C.E., and J.S. acknowledge the support of the EU grant QUANTIHEAT (project 604668). The authors acknowledge helpful scientific support and discussion of Jean-Christophe Charlier and Severine Gomez. P.G. and J.S. acknowledge financial support from the F.R.S.-FNRS of Belgium (FNRS-CQ-1.C044.21-SMARD, FNRS-CDR-J.0068.21-SMARD, FNRS-MIS-F.4523.22-TopoBrain, FNRS-PDR-T.0128.24-ART-MULTI, FNRS-CR-1.B.463.22-MouleFrits). P.G. acknowledges financial support from the EU (ERC-StG-10104144-MOUNTAIN), from the Federation Wallonie-Bruxelles through the ARC Grant No. 21/26-116, and from the FWO and FRS-FNRS under the Excellence of Science (EOS) program (40007563-CONNECT).

## DATA AVAILABILITY STATEMENT

The data that support the findings of this study are available from the corresponding author upon reasonable request.

[1] F. Sarvar, D. C. Whalley, and P. P. Conway, "Thermal interface materials-a review of the state of the art," in *2006 1st Electronic Systemintegration Technology Conference*, Vol. 2 (IEEE, 2006) pp. 1292–1302.

[2] K. M. Razeeb, E. Dalton, G. L. W. Cross, and A. J. Robinson, "Present and future thermal interface materials for electronic devices," International Materials Reviews **63**, 1–21 (2018).

[3] R. Prasher, "Thermal interface materials: historical perspective, status, and future directions," Proceedings of the IEEE **94**, 1571–1586 (2006).

[4] G. Yuan, H. Li, B. Shan, and J. Liu, "Thermal interface materials based on vertically aligned carbon nanotube arrays: a review," Micro and Nanosystems **11**, 3–10 (2019).

[5] L. Ping, P.-X. Hou, C. Liu, and H.-M. Cheng, "Vertically aligned carbon nanotube arrays as a thermal interface material," APL Materials **7**, 020902 (2019).

[6] S. Kaur, N. Raravikar, B. A. Helms, R. Prasher, and D. F. Ogletree, "Enhanced thermal transport at covalently functionalized carbon nanotube array interfaces," Nature communications **5**, 1–8 (2014).

[7] J. Xu and T. S. Fisher, "Enhancement of thermal interface materials with carbon nanotube arrays," International Journal of Heat and Mass Transfer **49**, 1658–1666 (2006).

[8] A. J. McNamara, Y. Joshi, and Z. M. Zhang, "Thermal resistance of thermal conductive adhesive anchored carbon nanotubes interface material," International Journal of Thermal Sciences **96**, 221–226 (2015).

[9] Y. Ni, H. Le Khanh, Y. Chalopin, J. Bai, P. Lebarny, L. Divay, and S. Volz, "Highly efficient thermal glue for carbon nanotubes based on azide polymers," Applied Physics Letters **100**, 193118 (2012).

[10] E. Pop, D. Mann, Q. Wang, K. Goodson, and H. Dai, "Thermal conductance of an individual single-wall carbon nanotube above room temperature," Nano letters **6**, 96–100 (2006).

[11] J. Hone, M. Whitney, C. Piskoti, and A. Zettl, "Thermal conductivity of single-walled carbon nanotubes," Physical Review B **59**, R2514 (1999).

[12]B. Kumanek and D. Janas, "Thermal conductivity of carbon nanotube networks: A review," Journal of Materials Science **54**, 7397–7427 (2019).
[13]T. Tong, Y. Zhao, L. Delzeit, A. Kashani, M. Meyyappan, and A. Majumdar, "Dense vertically aligned multiwalled carbon nanotube arrays as thermal interface materials," IEEE Transactions on Components and Packaging Technologies **30**, 92–100 (2007).
[14]Y. Xie, T. Wang, B. Zhu, C. Yan, P. Zhang, X. Wang, and G. Eres, "19-fold thermal conductivity increase of carbon nanotube bundles toward high-end thermal design applications," Carbon **139**, 445–458 (2018).
[15]Y. Feng, T. Inoue, H. An, R. Xiang, S. Chiashi, and S. Maruyama, "Quantitative study of bundle size effect on thermal conductivity of single-walled carbon nanotubes," Applied Physics Letters **112**, 191904 (2018).
[16]L. Shi, D. Li, C. Yu, W. Jang, D. Kim, Z. Yao, P. Kim, and A. Majumdar, "Measuring thermal and thermoelectric properties of one-dimensional nanostructures using a microfabricated device," J. Heat Transfer **125**, 881–888 (2003).
[17]A. J. Robson, I. Grishin, R. J. Young, A. M. Sanchez, O. V. Kolosov, and M. Hayne, "High-accuracy analysis of nanoscale semiconductor layers using beam-exit ar-ion polishing and scanning probe microscopy," Acs Applied Materials & Interfaces **5**, 3241–3245 (2013).
[18]J. Spièce, C. Evangeli, A. J. Robson, A. El Sachat, L. Haenel, M. I. Alonso, M. Garriga, B. J. Robinson, M. Oehme, J. Schulze, *et al.*, "Quantifying thermal transport in buried semiconductor nanostructures via cross-sectional scanning thermal microscopy," Nanoscale (2021).
[19]S. Gonzalez-Munoz, K. Agarwal, E. G. Castanon, Z. R. Kudrynskyi, Z. D. Kovalyuk, J. Spièce, O. Kazakova, A. Patanè, and O. V. Kolosov, "Direct measurements of anisotropic thermal transport in $\gamma$-inse nanolayers via cross-sectional scanning thermal microscopy," Advanced Materials Interfaces , 2300081 (2023).
[20]A. Nylander, J. Hansson, M. Kabiri Samani, C. Chandra Darmawan, A. Borta Boyon, L. Divay, L. Ye, Y. Fu, A. Ziaei, and J. Liu, "Reliability investigation of a carbon nanotube array thermal interface material," Energies **12**, 2080 (2019).
[21]K. Pandey, K. Paredis, A. J. Robson, and W. Vandervorst, "Understanding the effect of confinement in scanning spreading resistance microscopy measurements," Journal of Applied Physics **128**, 034303 (2020).
[22]H. Pan, Y. Chen, W. Pang, H. Sun, J. Li, Y. Lin, O. Kolosov, and Z. Huang, "Complementary sample preparation strategies (pvd/bexp) combining with multifunctional spm for the characterizations of battery interfacial properties," MethodsX **8**, 101250 (2021).
[23]O. Kolosov and K. Yamanaka, "Nonlinear detection of ultrasonic vibrations in an atomic force microscope," Japanese journal of applied physics **32**, L1095 (1993).
[24]B. J. Robinson, C. E. Giusca, Y. T. Gonzalez, N. D. Kay, O. Kazakova, and O. V. Kolosov, "Structural, optical and electrostatic properties of single and few-layers mos2: effect of substrate," 2D Materials **2**, 015005 (2015).
[25]A. Canetta, S. Gonzalez-Munoz, V.-H. Nguyen, K. Agarwal, P. d. C. de Picquendaele, Y. Hong, S. Mohapatra, K. Watanabe, T. Taniguchi, B. Nysten, *et al.*, "Quantifying the local mechanical properties of twisted double bilayer graphene," Nanoscale **15**, 8134–8140 (2023).
[26]A. El Sachat, J. Spiece, C. Evangeli, A. J. Robson, M. Kreuzer, M. R. Rodriguez-Laguna, E. Chavez, M. Sledzinska, C. M. Sotomayor Torres, O. V. Kolosov, *et al.*, "Nanoscale mapping of thermal and mechanical properties of bare and metal-covered self-assembled block copolymer thin films," ACS Applied Polymer Materials **2**, 487–496 (2019).
[27]J. Spiece, S. Sangtarash, M. Mucientes, A. J. Molina-Mendoza, K. Lulla, T. Mueller, O. Kolosov, H. Sadeghi, and C. Evangeli, "Low thermal conductivity in franckeite heterostructures," Nanoscale **14**, 2593–2598 (2022).
[28]C. Evangeli, J. Spiece, S. Sangtarash, A. J. Molina-Mendoza, M. Mucientes, T. Mueller, C. Lambert, H. Sadeghi, and O. Kolosov, "Nanoscale thermal transport in 2d nanostructures from cryogenic to room temperature," Advanced Electronic Materials **5**, 1900331 (2019).
[29]J. Spiece, C. Evangeli, K. Lulla, A. Robson, B. Robinson, and O. Kolosov, "Improving accuracy of nanothermal measurements via spatially distributed scanning thermal microscope probes," Journal of Applied Physics **124**, 015101 (2018).
[30]C. J. Glassbrenner and G. A. Slack, "Thermal conductivity of silicon and germanium from 3 k to the melting point," Physical review **134**, A1058 (1964).
[31]E. Guen, P.-O. Chapuis, R. Rajkumar, P. Dobson, G. Mills, J. Weaver, and S. Gomès, "Scanning thermal microscopy on samples of varying effective thermal conductivities and identical flat surfaces," Journal of Applied Physics **128**, 235301 (2020).
[32]J. S. Bulmer, A. Kaniyoor, and J. A. Elliott, "A meta-analysis of conductive and strong carbon nanotube materials," Advanced Materials **33**, 2008432 (2021).
[33]H.-Y. Chiu, V. Deshpande, H. C. Postma, C. Lau, C. Miko, L. Forro, and M. Bockrath, "Ballistic phonon thermal transport in multiwalled carbon nanotubes," Physical review letters **95**, 226101 (2005).
[34]Q. Zhang, G. Chen, S. Yoon, J. Ahn, S. Wang, Q. Zhou, Q. Wang, J. Li, *et al.*, "Thermal conductivity of multiwalled carbon nanotubes," Physical Review B **66**, 165440 (2002).
[35]P. Kim, L. Shi, A. Majumdar, and P. L. McEuen, "Thermal transport measurements of individual multiwalled nanotubes," Physical review letters **87**, 215502 (2001).
[36]A. M. Marconnet, M. A. Panzer, and K. E. Goodson, "Thermal conduction phenomena in carbon nanotubes and related nanostructured materials," Reviews of Modern Physics **85**, 1295 (2013).
[37]M. E. Siemens, Q. Li, R. Yang, K. A. Nelson, E. H. Anderson, M. M. Murnane, and H. C. Kapteyn, "Quasi-ballistic thermal transport from nanoscale interfaces observed using ultrafast coherent soft x-ray beams," Nature materials **9**, 26–30 (2010).
[38]T. Yamamoto, S. Konabe, J. Shiomi, and S. Maruyama, "Crossover from ballistic to diffusive thermal transport in carbon nanotubes," Applied Physics Express **2**, 095003 (2009).
[39]N. Mingo and D. Broido, "Length dependence of carbon nanotube thermal conductivity and the "problem of long waves"," Nano letters **5**, 1221–1225 (2005).
[40]C. Yu, L. Shi, Z. Yao, D. Li, and A. Majumdar, "Thermal conductance and thermopower of an individual single-wall carbon nanotube," Nano letters **5**, 1842–1846 (2005).
[41]K. Kim, W. Jeong, W. Lee, and P. Reddy, "Ultra-high vacuum scanning thermal microscopy for nanometer resolution quantitative thermometry," Acs Nano **6**, 4248–4257 (2012).
[42]Y. Muzychka, M. Yovanovich, and J. Culham, "Thermal spreading resistance in compound and orthotropic systems," Journal of thermophysics and heat transfer **18**, 45–51 (2004).
[43]F. Menges, H. Riel, A. Stemmer, C. Dimitrakopoulos, and B. Gotsmann, "Thermal transport into graphene through nanoscopic contacts," Physical review letters **111**, 205901 (2013).
[44]Y.-K. Kwon and P. Kim, "Unusually high thermal conductivity in carbon nanotubes," in *High Thermal Conductivity Materials* (Springer, 2006) pp. 227–265.
[45]C. Zhang, Y. Song, H. Zhang, B. Lv, J. Qiao, N. Yu, Y. Zhang, J. Di, and Q. Li, "Mechanical properties of carbon nanotube fibers at extreme temperatures," Nanoscale **11**, 4585–4590 (2019).
[46]I.-K. Hsu, M. T. Pettes, A. Bushmaker, M. Aykol, L. Shi, and S. B. Cronin, "Optical absorption and thermal transport of individual suspended carbon nanotube bundles," Nano Letters **9**, 590–594 (2009).
[47]J. Che, T. Cagin, and W. A. Goddard III, "Thermal conductivity of carbon nanotubes," Nanotechnology **11**, 65 (2000).
[48]W. J. Evans, M. Shen, and P. Keblinski, "Inter-tube thermal conductance in carbon nanotubes arrays and bundles: Effects of contact area and pressure," Applied Physics Letters **100**, 261908 (2012).